Supplement for: Increasing Sea Surface Temperature Suppresses Primary Marine Aerosol Production

Raymond J. Leibensperger III[1,†,+], Justin D. Hamlin[2,†], Jena K. Herbst[1], Charbel Harb[1,‡], Ke'La A. Kimble[2,§], Meinrat O. Andreae[1,3], Christopher Lee[1], Greg Sandstrom[1], M. Dale Stokes[1], Grant B. Deane[1], Kimberly A. Prather[1,2,*]

[1]Scripps Institution of Oceanography, University of California San Diego, La Jolla, CA, USA
[2]Department of Chemistry and Biochemistry, University of California San Diego, La Jolla, CA, USA
[3]Max Planck Institute for Chemistry, Mainz, Germany
[†]These authors contributed equally to this work
[+]Now at: Institute of Environmental Physics, Heidelberg University, Heidelberg, Germany
[‡]Now at: RTI International, Durham, NC, USA
[§]Now at: California Air Resources Board, Sacramento, CA, USA

Correspondence to: Kimberly A. Prather (kprather@ucsd.edu)

S1 Previous Literature

The dependence of sea spray aerosol (SSA) production on sea surface temperature (SST) has long been investigated in the laboratory and field. To target specific processes and elements of this complicated relationship, laboratory studies have used a variety of wave breaking analogues, complicating the comparisons of findings. A summary of previous studies is included in Table S1. Of the 19 previous studies encompassing 22 independent SSA-SST relationships, seven identified a positive dependence, eight identified a negative dependence, and seven identified a non-monotonic dependence.

	Reference	Study Type	Wave Breaking Analog	SSA-SST Dependence
1	Callaghan et al. (2014)	Laboratory	MART	Positive
2	Christiansen et al. (2019)	Laboratory	Plunging Jet Diffuser	Jet: Non-monotonic Diffuser: Negative
3	Forestieri et al. (2018)	Laboratory	miniMART	Positive
4	Hu et al. (2024)	Laboratory	Plunging Jet Plunging Waterfall	Jet: Non-monotonic Waterfall: Positive
5	Mårtensson et al. (2003)	Laboratory	Sintered Glass Filter	Non-monotonic
6	Nielsen & Bilde (2020)	Laboratory	Pipette Bubbler	Negative
7	Salter et al. (2014)	Laboratory	Plunging Jet	Negative
8	Salter et al. (2015)	Laboratory	Plunging Jet	Negative
9	Sellegri et al. (2023)	Laboratory	Plunging Jet	Negative
10	Sofieva et al. (2022)	Laboratory	Diffuser	Non-monotonic
11	Zábori et al. (2012)	Laboratory	Plunging Jet	Non-monotonic
12	Zinke et al. (2022)	Laboratory	N/A	Non-monotonic
13	Grythe et al. (2014)	Field	N/A	Positive
14	Jaeglé et al. (2011)	Field	N/A	Non-monotonic
15	Lehahn et al. (2014)	Field	N/A	Negative
16	Liu et al. (2021)	Field	N/A	Positive

17	Markuszewski et al. (2024)	Field	N/A	Negative
18	Ovadnevaite et al. (2014)	Field	N/A	Positive
19	Saliba et al. (2019)	Field	N/A	Number: Negative Mass: Positive
20	**This study**	**Laboratory**	**Wind-Wave Interactions (SOARS)**	**Submicron: Negative** **Supermicron: Non-monotonic**

Table S1: Summary of previously documented SSA-SST relationships and method of investigation.

S2 Experimental Conditions

Experimental Summary		Channel Conditions		SSA Sample Conditions	
		SST Range	Salinity	RH	Flow Rate
Experiment	Dates	[°C]	[PSU]	[%]	[L min^{-1}]
Cooling	11 - 16 February 2024	2.2 - 20.0	36.4 ± 0.2	19 ± 4	6.2[a] 2.6[b]
Warming	17 February - 01 March 2024	2.5 - 23	36.2 ± 0.2	20 ± 3	6.2[a] 2.6[b]

Table S2: Summary of experimental conditions. Both experiments were conducted with filtered seawater filled to a channel depth of 1.2 m. Wind speed was 11 m s^{-1}. Wave stroke height was 0.42 m. [a] Sampling system consisting of 2x SMPS and 1x APS. [b] Sampling system consisting of SM, OPS, MAGIC CPC, NanoScan SMPS.

Sea spray aerosol (SSA) particle number size distributions (PNSDs) are reported for equilibrium wind-wave conditions in SOARS. SOARS includes two makeup fans that maintain positive pressure within the channel and minimize room air contamination. To account for background aerosol concentrations and ensure minimal contamination, PNSDs were measured during each period shown in **Error! Reference source not found.**b in the main text. PNSDs of each period were measured across three days, each with an SST of 20 °C (Figure S1a-c). Multi-day mean PNSDs for each period are exhibited in Figure S1d and probability density functions (PDFs) of the multi-day mean PNSDs are shown in Figure S1e, demonstrating that Wind & Waves is distinct from the other events. The PNSDs observed during Wind & Waves have a similar bimodal shape as other laboratory measurements of SSA (Prather et al., 2013; Stokes et al., 2013). The remaining events, Room Air, Aerosol Mode, and Wind Alone show higher variability. This highlights two features: (1) SOARS's precision in generating SSA under wind-wave interactions (relative standard deviation of ~20% compared to ~50% for other conditions) and (2) that the SSA population produced by SOARS is minimally influenced by contamination. Further discussion of SSA measurement considerations is provided in Sect. S5.

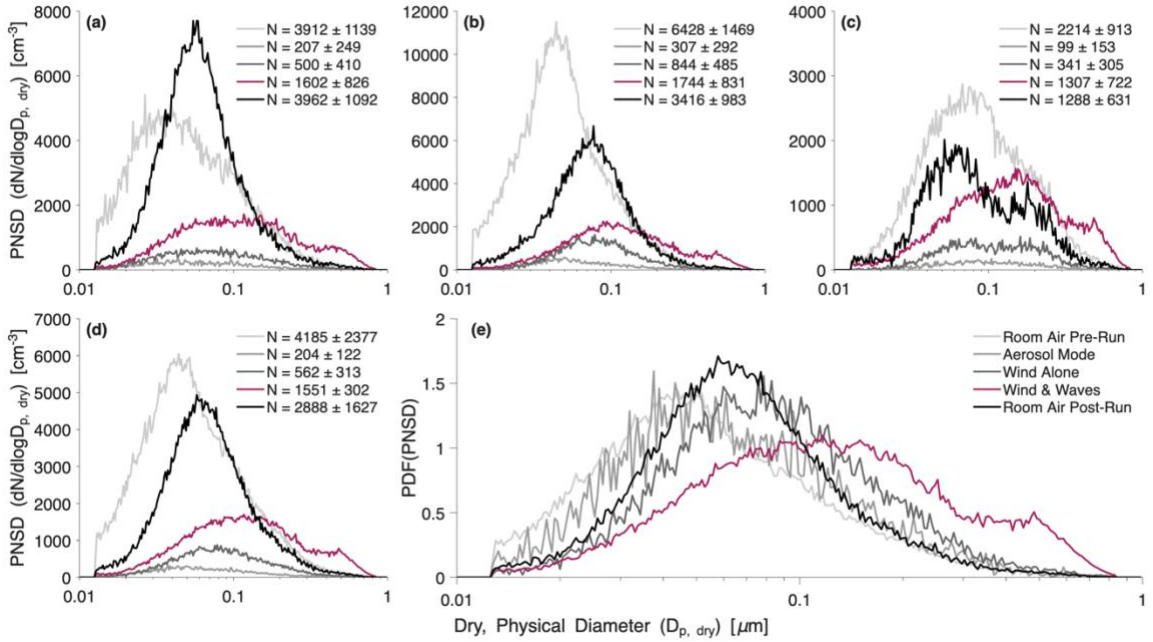

Figure S1: (a) Condition-averaged PNSDs for cooling experiment day 1, (b) cooling experiment day 2, and (c) warming experiment day 5. (d) 3-day average PNSDs across SOARS events. (e) Probability density function (PDF) of 3-day average PNSDs across SOARS events. Total number concentrations ± 1 standard deviation are shown in (a-d).

S3 Sea Spray Aerosol Sampling & Corrections

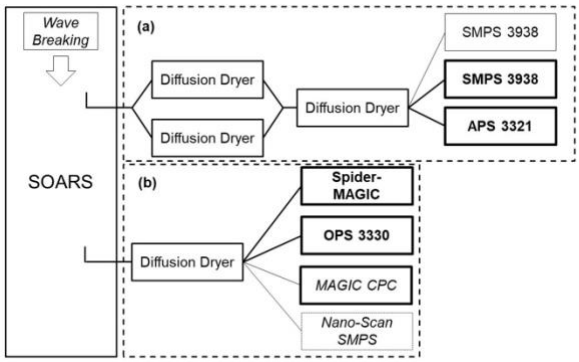

Figure S2: Sampling schematic. (a) Primary instruments and (b) secondary instruments. The sampling inlet of the secondary instruments (b) was positioned 2 m downstream of the primary instruments (a). Sampling lines were constructed of stainless steel and black conductive tubing. Sample inlets were positioned in the direction of wave breaking to achieve near-isoaxial sampling.

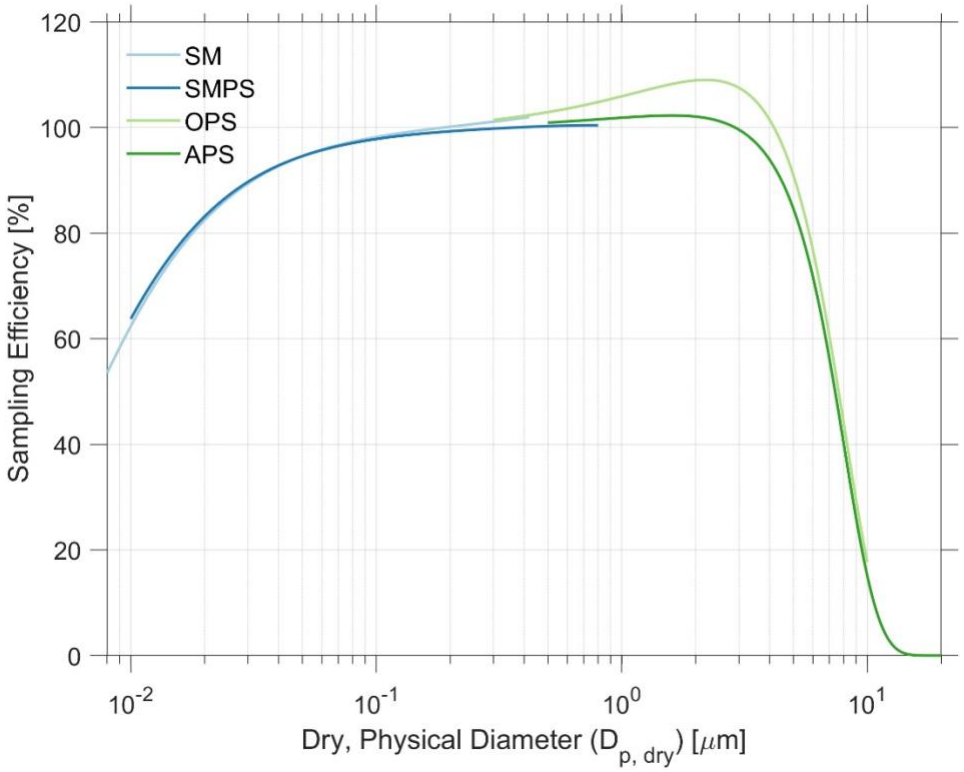

Figure S3: Sampling efficiency determined using the Particle Loss Calculator (PLC, Von Der Weiden et al., (2009)) for the aerosol sampling instruments used in this study.

S4 Measurement Considerations

SOARS allows for extensive controls of experimental variables; however, achieving SSTs near the upper and lower limits of its operational limit was time-intensive, reducing the number of data points achieved at the lowest and highest SSTs. Weighted least squares regressions were applied to reduce the influence of the number of runs within each SST bin. The weighting factor (w) is equal to the inverse of the measurement variance (σ^2):

$$\boldsymbol{w = \frac{1}{\sigma^2}}, \quad \textbf{(S1)}$$

The influence of weighted and unweighted least squares regressions is shown in Figure S4. Non-weighted regressions show high coefficients of determination ($R^2 \geq 0.92$) for both linear and quadratic models, except for the supermicron linear model. Weighted least squares regression shows a slight improvement in performance due to the higher uncertainty associated with measurements at moderate SSTs (i.e., between 5 and 15 °C). The weighting process was applied to the PNFDs and PMFDs in the main text.

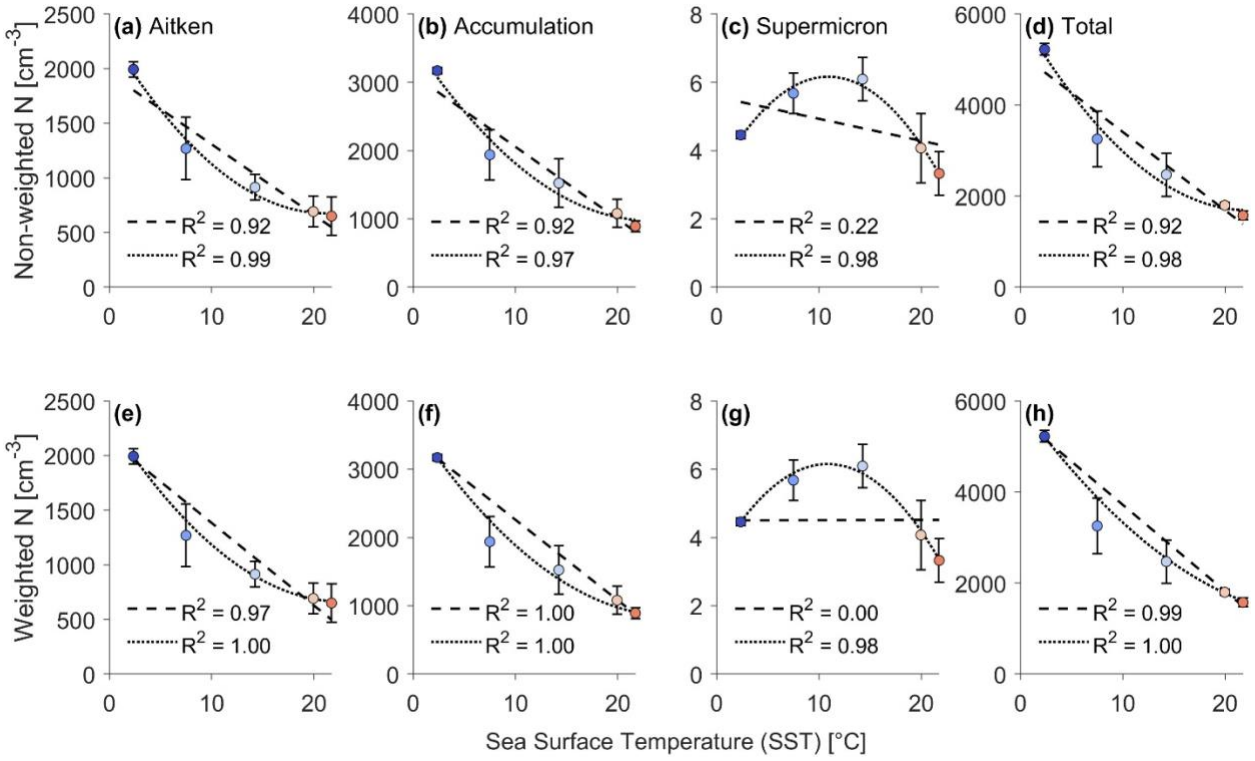

Figure S4: (top row) Non-weighted least squares regression based on Aitken, Accumulation, Supermicron and total number concentrations. (bottom row) Same as top row but weighted using Eq. S1. Linear models are shown by dashed lines, and quadratic models are shown by dotted lines.

S5 Theoretical Framework

The framework described in the main text relies on known quantities of subsurface bubbles (n) and surface bubbles (ñ) to estimate the net number of SSA of a given $D_{p,\,dry}$ that enters the atmosphere per square meter of ocean surface (N). Equation 4 summarizes the dependence of N on n and ñ, which are also time dependent. Equations S1 and S2 describe their change in concentrations:

$$\frac{d\tilde{n}}{dt} = Z * R * n - (B + C + D_2) * \tilde{n}, \quad \text{(S2)}$$

$$\frac{dn}{dt} = F - (R + D_3) * n, \quad \text{(S3)}$$

Where Z is the depth of the subsurface bubble plume [m], R is the rate of breeching of subsurface bubbles on the surface [s^{-1}], C encompasses the rate of the net effects of surface bubble coalescence [s^{-1}], D_2 is the rate of dissolution of surface bubbles [s^{-1}], F is a function describing the formation of subsurface bubbles [$\#_{bubble}\ m^{-3}\ \mu m^{-1}\ s^{-1}$], and D_3 is the rate of subsurface bubbles lost to dissolution and removal [s^{-1}].

Equations S1 and S2 can be rearranged for ñ and n, respectively, which can then be substituted into Eq. 4 to solve for $\frac{dN}{dt}$. However, this method of solving the equations relies on knowledge of the concentration changes over time ($\frac{d\tilde{n}}{dt}$ & $\frac{dn}{dt}$), which can be determined experimentally.

Similar to Eqs. 5 and 6, here we document the dependencies of terms of Eqs. S1-S2 on SST. The rate at which subsurface bubbles breach the ocean surface (R) is known to be proportional to surface tension (γ) and inversely proportional to viscosity (ν) and solubility (κ) (Jaeglé et al., 2011; Nielsen and Bilde, 2020; Ovadnevaite et al., 2014; Sellegri et al., 2023; Song et al., 2023; Zábori et al., 2012):

$$R \propto \frac{\gamma}{\nu\kappa}, \quad \text{(S4)}$$

Surface bubble coalescence (C) could be positive or negative, depending on the net effects of combining bubbles and shifting the bubble size distribution. C is expected to be primarily related to the size and number of surface bubbles, the area over which they extend, and γ holding bubbles together:

$$C \propto \gamma^{-1}, \quad \text{(S5)}$$

The rate of subsurface bubbles lost to dissolution and removal (D_3) and the rate of dissolution of surface bubbles (D_2) are expected to be proportional to solubility (κ) and viscosity (ν), but inversely proportional to surface tension (γ) (Song et al., 2023; Zábori et al., 2012). Additionally, surface bubble dissolution is likely to be small, instead favouring bubble coalescence or bursting.

$$D_2 \propto \frac{\kappa\nu}{\gamma} \ll 1, \quad \text{(S6)}$$

$$D_3 \propto \frac{\kappa\nu}{\gamma}, \quad \text{(S7)}$$

The subsurface bubble formation rate is proportional to air entrainment (ε) (Callaghan et al., 2014):

$$F \propto \varepsilon, \quad \text{(S8)}$$

S6 Particle Number Size Distributions

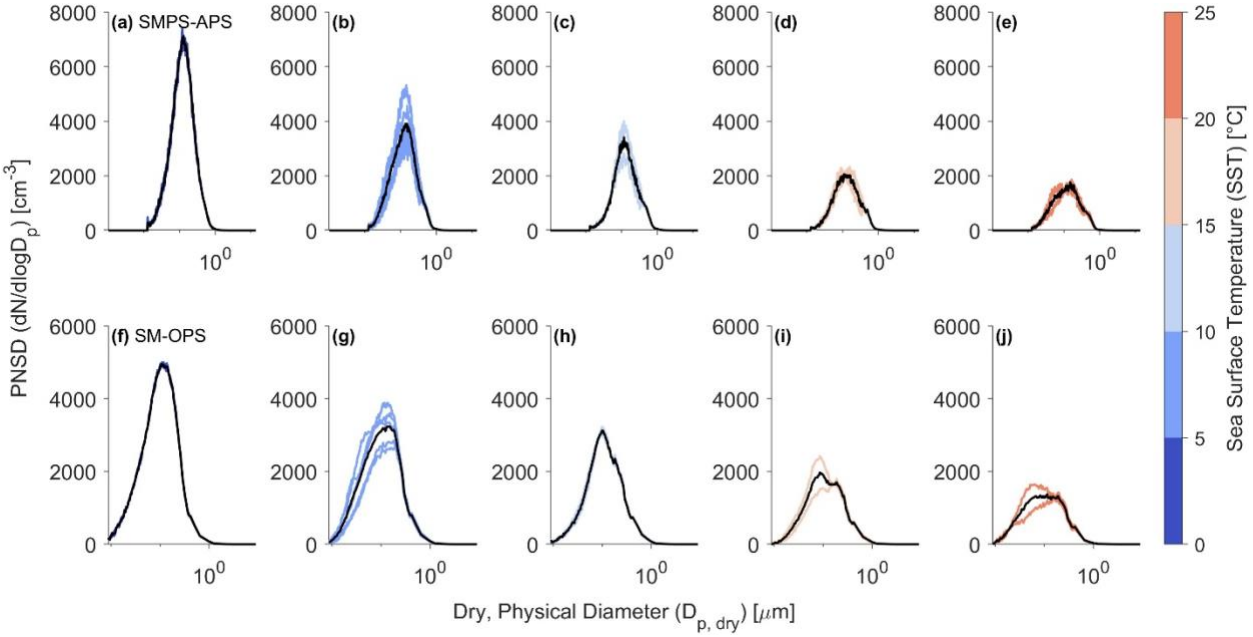

Figure S5: Steady-state PNSDs for each SST experimental run across five ranges:(right to left) 0-5 °C, 5-10 °C, 10-15 °C, 15-20 °C, 20-25 °C. (top row) SMPS-APS measurements and (bottom row) SM-OPS measurements. Mean PNSDs for each SST range are shown by a black line.

SST [°C]	D_g [µm]		σ_g		D_{mode} [µm]		N [cm^{-3}]	
-	SMPS-APS	SM-OPS	SMPS-APS	SM-OPS	SMPS-APS	SM-OPS	SMPS-APS	SM-OPS
2.4 ± 0.2	0.1119 ± 0.0011	0.0938 ± 0.0003	1.97 ± 0.02	2.216 ± 0.001	0.1343 ± 0.0011	0.116 ± 0.004	5222 ± 127	4289.1 ± 0.4
8 ± 2	0.110 ± 0.008	0.096 ± 0.009	2.06 ± 0.04	2.28 ± 0.04	0.142 ± 0.008	0.129 ± 0.014	3254 ± 613	3212 ± 527
14.25 ± 0.07	0.114 ± 0.005	0.104 ± 0.003	1.98 ± 0.04	2.168 ± 0.019	0.1185 ± 0.0011	0.103 ± 0.004	2471 ± 476	2534 ± 85
19.95 ± 0.07	0.112 ± 0.017	0.104 ± 0.015	2.04 ± 0.02	2.202 ± 0.003	0.136 ± 0.042	0.13 ± 0.05	1798 ± 61	1828 ± 309
22 ± 2	0.104 ± 0.014	0.091 ± 0.003	2.162 ± 0.005	2.40 ± 0.11	0.134 ± 0.044	0.11 ± 0.05	1576 ± 96	1514 ± 332

Table S3: Summary of binned results. An additional significant digit is retained when the last significant digit is 1.

id

S7 Parameters of the Particle Number Size Distribution

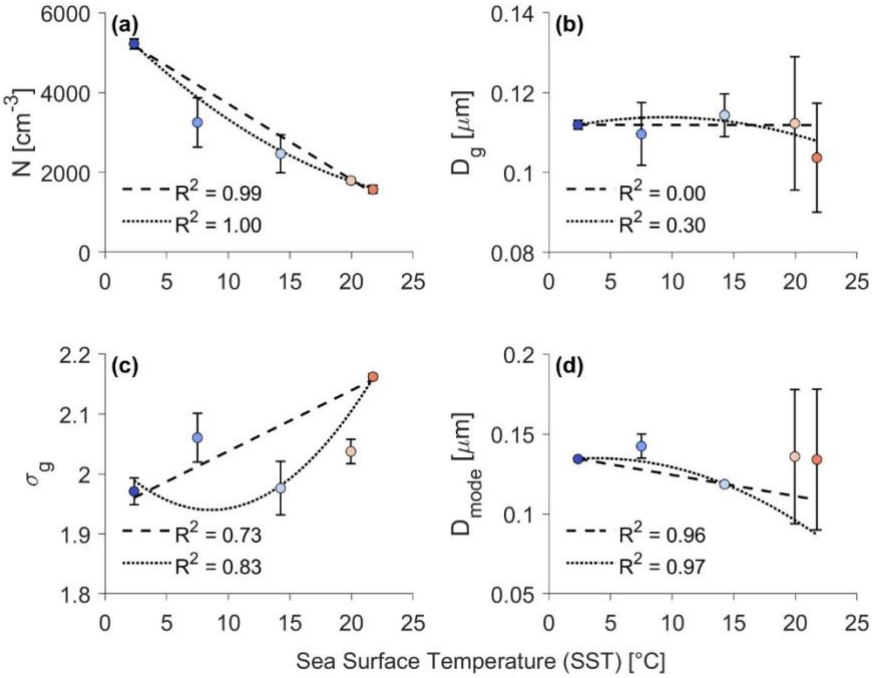

Figure S6: Key parameters of the particle number size distribution: (a) total number concentration, N, (b) geometric mean diameter, D_g, (c) geometric standard deviation, σ_g, and (d) mode diameter, D_{mode}. Linear (dashed) and quadratic (dotted) best-fit lines are shown in each panel. Error bars represent 1 standard deviation.

S8 Sea Spray Aerosol Mode Fitting

Aerosol size distributions have been previously described by a tri-modal scheme (Dedrick et al., 2024; Modini et al., 2015; Williams et al., 2024). Here, we separate the PNSDs, PNFDs, and PMFDs at the extreme temperatures in a tri-modal scheme comprised of the Aitken (≤ 0.1 μm), accumulation (0.1-1 μm), and supermicron (≥ 1 μm) modes as described in the main text. Table S4 describes the results of tri-modal fitting on the lowest (0-5 °C) and highest (20-25 °C) SST bins.

SST [°C]	Aitken			Accumulation			Supermicron		
PNSD	**N [cm^{-3}]**	**D_g [μm]**	**σ_g**	**N [cm^{-3}]**	**D_g [μm]**	**σ_g**	**N [cm^{-3}]**	**D_g [μm]**	**σ_g**
0-5	500	0.038	1.65	4468	0.130	1.82	142	0.416	1.61
20-25	325	0.046	1.71	1132	0.154	1.83	91	0.423	1.68
Difference	-175	0.008	0.06	-3336	0.024	0.02	-51	0.007	0.07
PNFD	**F_N [m^{-2} s^{-1}]**	**D_g [μm]**	**σ_g**	**F_N [m^{-2} s^{-1}]**	**D_g [μm]**	**σ_g**	**F_N [m^{-2} s^{-1}]**	**D_g [μm]**	**σ_g**

0-5	5.613e6	0.055	1.80	5.009e6	0.171	1.80	3.995e5	0.800	1.55
20-25	1.010e6	0.043	1.40	2.090e6	0.151	1.83	1.772e6	0.800	1.54
Difference	-4.603e6	-0.012	-0.40	-2.919e6	-0.021	0.03	1.373e6	0	-0.02
PMFD	**F_M [m^3 m^{-2} s^{-1}]**	**D_g [µm]**	**σ_g**	**F_M [m^3 m^{-2} s^{-1}]**	**D_g [µm]**	**σ_g**	**F_M [m^3 m^{-2} s^{-1}]**	**D_g [µm]**	**σ_g**
0-5	3.094e-6	0.068	1.80	8.175e-4	0.360	1.80	0.0058	1.073	1.66
20-25	1.639e-7	0.035	1.32	6.028e-5	0.199	1.60	0.0157	1.542	1.76
Difference	-2.930e-6	-0.033	-0.48	-7.572e-4	-0.161	-0.20	0.0099	0.471	0.10

Table S4: Magnitude, geometric mean diameter, and geometric standard deviation information for tri-modal fitting to temperature extremes PNSDs, PNFDs, and PMFDs.

S9 Higher-Order Size Distributions

Laboratory measurements of SSA are influenced by the breaking wave proxy. In this study, SOARS was operated with continuously recirculating winds, unlike previous studies, which employed flow-through systems (Christiansen et al., 2019; Hu et al., 2024; Sauer et al., 2022). A thorough analysis comparing flow-through and well-mixed SSA generators is beyond the scope of this work, so we provide probability density functions (PDF) of measured size distributions (Figure S7) to aid in comparisons to other breaking wave proxies. Particle number, surface area, and volume size distributions can be reconstructed by the interested reader using the total number, surface area, and volume estimates included in the legends. The prevalence of the secondary mode at the warmest SSTs accounts for the differences in PDF shapes.

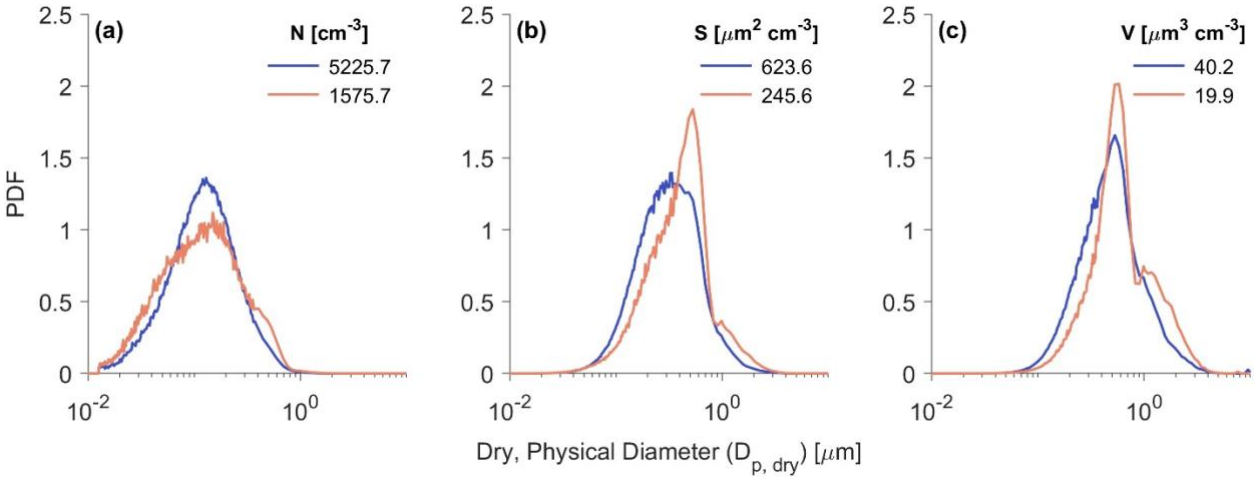

Figure S7: PDF of (a) number, (b) surface area, and (c) volume size distributions at the lowest and highest SST. PDFs are normalized by the total concentrations indicated in each respective legend.

Sea spray aerosols are the largest natural source of aerosol mass, and changing sea surface temperature, as shown here, will have profound effects on Earth's climate (Grythe et al., 2014; de Leeuw et al., 2011; Lewis and Schwartz, 2004). Figure S8 demonstrates that shifts in SST will have size-dependent effects on the mass of SSA produced.

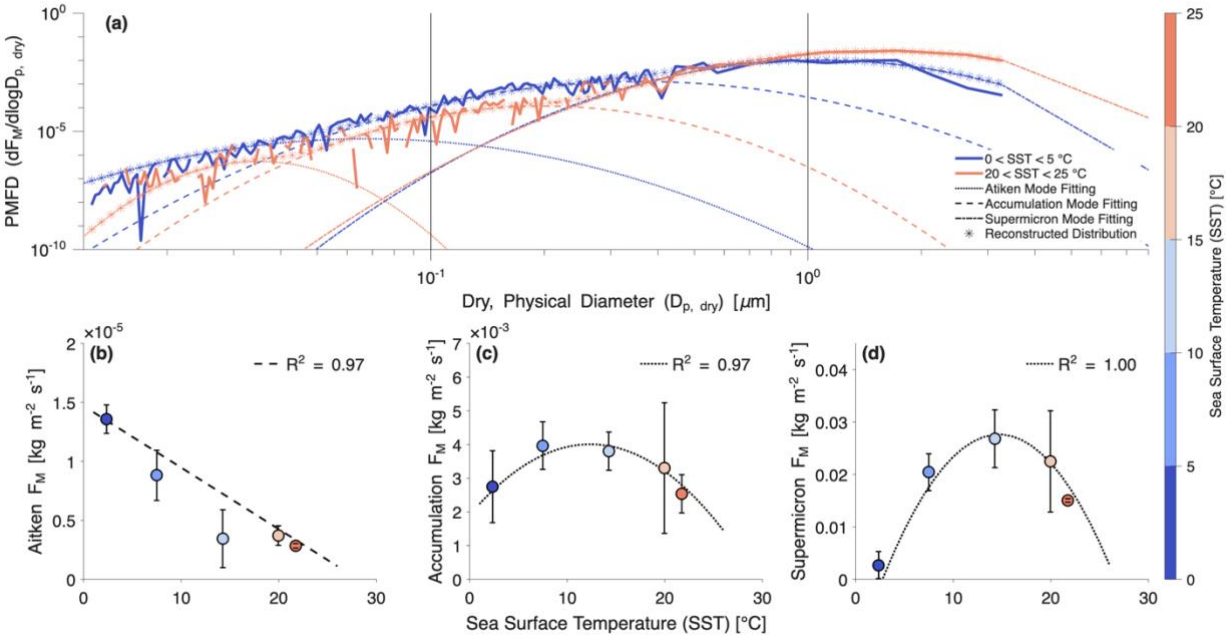

Figure S8: Particle mass flux distributions (a) for the warmest and coldest SST bins. Accompanying mode fitting included. Total mass flux as a function of SST for Aitken mode (b), accumulation mode (c), and supermicron (d) SSA.

S10 Experiment Comparisons

The analysis and figures of the main text condense measurements across the two experiments for simplicity and to account for the daily variability of the system. The dependencies of modal number flux (F_N) and mass flux (F_M) are included here, separated into Aitken, accumulation, and supermicron modes, along with total flux. They are also separated into the cooling experiment, the warming experiment, and combined. Figure S9 showcases the separation of number flux and Figure S10 showcases the separation of mass flux. In the combined column (panels c, f, i, and l) of each figure, the temperature-binned estimates are overlaid, and the best-fit line from the main text figures is included as a bolded line. It is important to note that the R^2 value for the temperature-binned data is close to 1 due to the limited number of input data points (n = 5), however, the regression of the temperature-binned data closely aligns with the regression of the combined data points from both experiments (n = 13). While the regressions and figures in the main text are simplified versions to aid in clarity, they represent the trends well despite the low number of input data points.

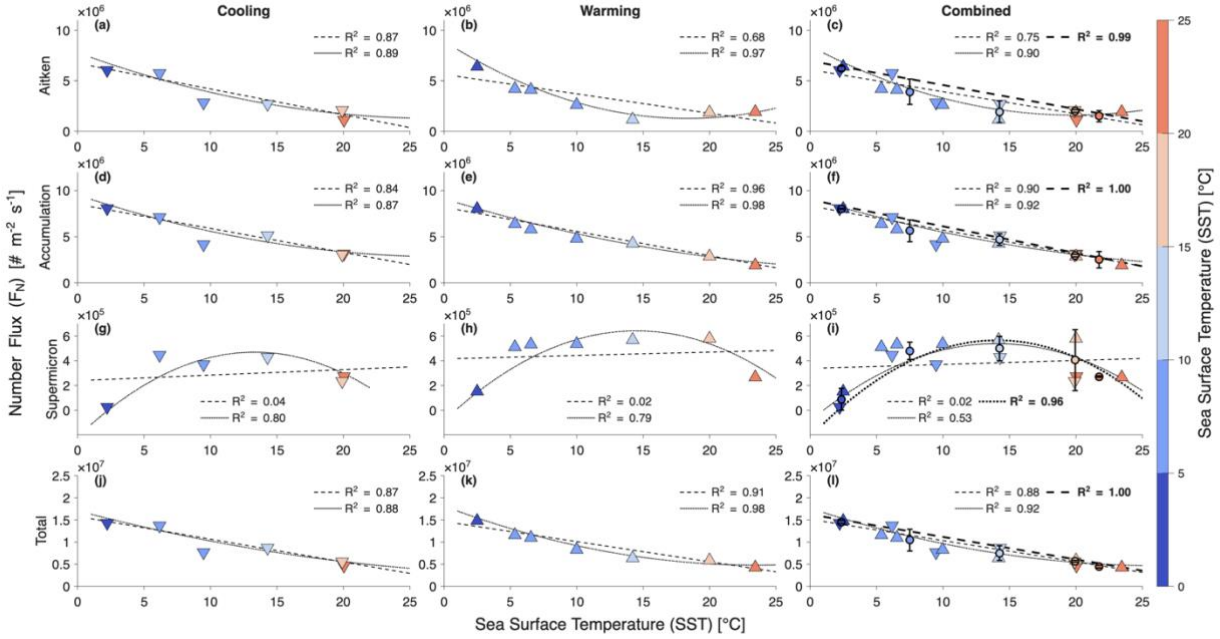

Figure S9: Total number flux (F_N) by experiment (columns) and size range (rows). Dashed lines indicate linear regressions, and dotted lines indicate quadratic regressions. The recommended regression based on temperature-binned data is included in panels c, f, i, and l as bolded lines.

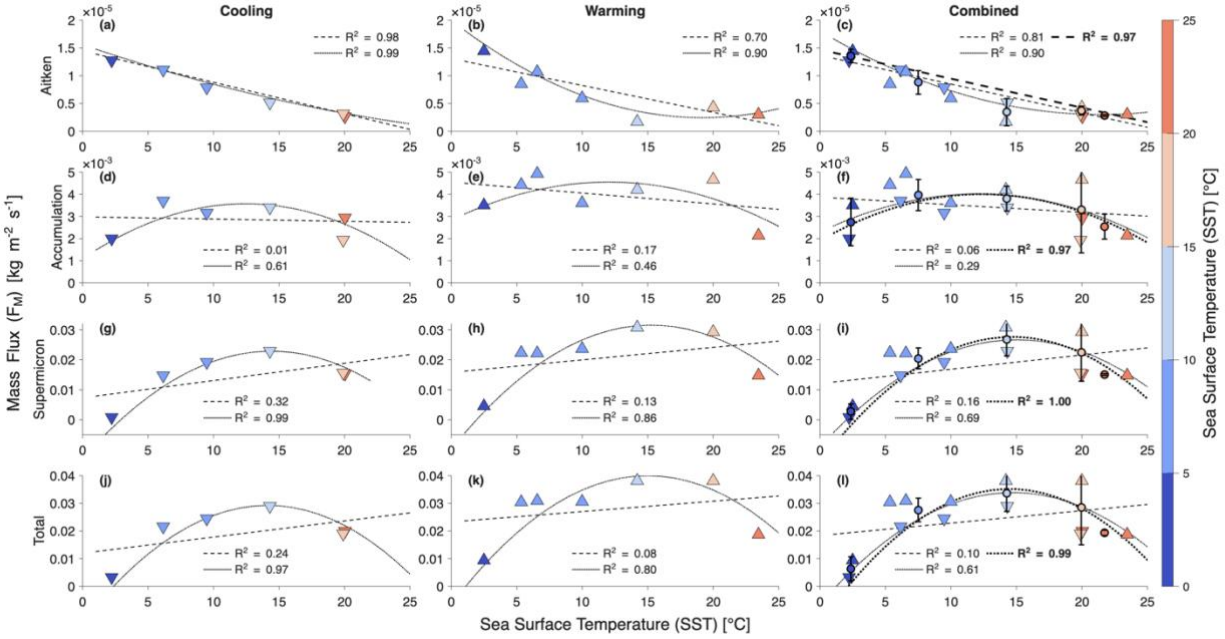

Figure S10: Total mass flux (F_M) by experiment (columns) and size range (rows). Dashed lines indicate linear regressions, and dotted lines indicate quadratic regressions. The recommended regression based on temperature-binned data is included in panels c, f, i, and l as bolded lines.

References

Callaghan, A. H., Stokes, M. D., and Deane, G. B.: The effect of water temperature on air entrainment, bubble plumes, and surface foam in a laboratory breaking-wave analog, Journal of Geophysical Research: Oceans, 119, 7463–7482, https://doi.org/10.1002/2014JC010351, 2014.

Christiansen, S., Salter, M. E., Gorokhova, E., Nguyen, Q. T., and Bilde, M.: Sea Spray Aerosol Formation: Laboratory Results on the Role of Air Entrainment, Water Temperature, and Phytoplankton Biomass, Environ. Sci. Technol., 53, 13107–13116, https://doi.org/10.1021/acs.est.9b04078, 2019.

Dedrick, J. L., Russell, L. M., Sedlacek III, A. J., Kuang, C., Zawadowicz, M. A., and Lubin, D.: Aerosol-Correlated Cloud Activation for Clean Conditions in the Tropical Atlantic Boundary Layer During LASIC, Geophysical Research Letters, 51, e2023GL105798, https://doi.org/10.1029/2023GL105798, 2024.

Forestieri, S. D., Moore, K. A., Martinez Borrero, R., Wang, A., Stokes, M. D., and Cappa, C. D.: Temperature and Composition Dependence of Sea Spray Aerosol Production, Geophysical Research Letters, 45, 7218–7225, https://doi.org/10.1029/2018GL078193, 2018.

Grythe, H., Ström, J., Krejci, R., Quinn, P., and Stohl, A.: A review of sea-spray aerosol source functions using a large global set of sea salt aerosol concentration measurements, Atmospheric Chemistry and Physics, 14, 1277–1297, https://doi.org/10.5194/acp-14-1277-2014, 2014.

Hu, J., Li, J., Tsona Tchinda, N., Song, Y., Xu, M., Li, K., and Du, L.: Underestimated role of sea surface temperature in sea spray aerosol formation and climate effects, npj Clim Atmos Sci, 7, 1–12, https://doi.org/10.1038/s41612-024-00823-x, 2024.

Jaeglé, L., Quinn, P. K., Bates, T. S., Alexander, B., and Lin, J.-T.: Global distribution of sea salt aerosols: new constraints from in situ and remote sensing observations, Atmospheric Chemistry and Physics, 11, 3137–3157, https://doi.org/10.5194/acp-11-3137-2011, 2011.

de Leeuw, G., Andreas, E. L., Anguelova, M. D., Fairall, C. W., Lewis, E. R., O'Dowd, C., Schulz, M., and Schwartz, S. E.: Production flux of sea spray aerosol, Reviews of Geophysics, 49, https://doi.org/10.1029/2010RG000349, 2011.

Lehahn, Y., Koren, I., Rudich, Y., Bidle, K. D., Trainic, M., Flores, J. M., Sharoni, S., and Vardi, A.: Decoupling atmospheric and oceanic factors affecting aerosol loading over a cluster of mesoscale North Atlantic eddies, Geophysical Research Letters, 41, 4075–4081, https://doi.org/10.1002/2014GL059738, 2014.

Lewis, E. R. and Schwartz, S. E.: Sea Salt Aerosol Production Mechanisms, Methods, Measurements and Models, Washington DC, 2004.

Liu, S., Liu, C. C., Froyd, K. D., Schill, G. P., Murphy, D. M., Bui, T. P., Dean-Day, J. M., Weinzierl, B., Dollner, M., Diskin, G. S., Chen, G., and Gao, R. S.: Sea spray aerosol concentration modulated by sea surface temperature, Proceedings of the National Academy of Sciences of the United States of America, 118, 3–8, https://doi.org/10.1073/pnas.2020583118, 2021.

Markuszewski, P., Nilsson, E. D., Zinke, J., Mårtensson, E. M., Salter, M., Makuch, P., Kitowska, M., Niedźwiecka-Wróbel, I., Drozdowska, V., Lis, D., Petelski, T., Ferrero, L., and Piskozub, J.: Multi-year gradient measurements of sea spray fluxes over the Baltic Sea and the North Atlantic Ocean, Atmospheric Chemistry and Physics, 24, 11227–11253, https://doi.org/10.5194/acp-24-11227-2024, 2024.

Mårtensson, E. M., Nilsson, E. D., de Leeuw, G., Cohen, L. H., and Hansson, H.-C.: Laboratory simulations and parameterization of the primary marine aerosol production, Journal of Geophysical Research: Atmospheres, 108, https://doi.org/10.1029/2002JD002263, 2003.

Modini, R. L., Frossard, A. A., Ahlm, L., Russell, L. M., Corrigan, C. E., Roberts, G. C., Hawkins, L. N., Schroder, J. C., Bertram, A. K., Zhao, R., Lee, A. K. Y., Abbatt, J. P. D., Lin, J., Nenes, A., Wang, Z., Wonaschütz, A., Sorooshian, A., Noone, K. J., Jonsson, H., Seinfeld, J. H., Toom-Sauntry, D., Macdonald, A. M., and Leaitch, W. R.: Primary marine aerosol-cloud interactions off the coast of California, Journal of Geophysical Research: Atmospheres, 120, 4282–4303, https://doi.org/10.1002/2014JD022963, 2015.

Nielsen, L. S. and Bilde, M.: Exploring controlling factors for sea spray aerosol production: temperature, inorganic ions and organic surfactants, Tellus B: Chemical and Physical Meteorology, 72, 1–10, https://doi.org/10.1080/16000889.2020.1801305, 2020.

Ovadnevaite, J., Manders, A., de Leeuw, G., Ceburnis, D., Monahan, C., Partanen, A.-I., Korhonen, H., and O'Dowd, C. D.: A sea spray aerosol flux parameterization encapsulating wave state, Atmos. Chem. Phys., 14, 1837–1852, https://doi.org/10.5194/acp-14-1837-2014, 2014.

Prather, K. A., Bertram, T. H., Grassian, V. H., Deane, G. B., Stokes, M. D., DeMott, P. J., Aluwihare, L. I., Palenik, B. P., Azam, F., Seinfeld, J. H., Moffet, R. C., Molina, M. J., Cappa, C. D., Geiger, F. M., Roberts, G. C., Russell, L. M., Ault, A. P., Baltrusaitis, J., Collins, D. B., Corrigan, C. E., Cuadra-Rodriguez, L. A., Ebben, C. J., Forestieri, S. D., Guasco, T. L., Hersey, S. P., Kim, M. J., Lambert, W. F., Modini, R. L., Mui, W., Pedler, B. E., Ruppel, M. J., Ryder, O. S., Schoepp, N. G., Sullivan, R. C., and Zhao, D.: Bringing the ocean into the laboratory to probe the chemical complexity of sea spray aerosol,

Proceedings of the National Academy of Sciences of the United States of America, 110, 7550–7555, https://doi.org/10.1073/pnas.1300262110, 2013.

Saliba, G., Chen, C.-L., Lewis, S., Russell, L. M., Rivellini, L.-H., Lee, A. K. Y., Quinn, P. K., Bates, T. S., Haëntjens, N., Boss, E. S., Karp-Boss, L., Baetge, N., Carlson, C. A., and Behrenfeld, M. J.: Factors driving the seasonal and hourly variability of sea-spray aerosol number in the North Atlantic, Proceedings of the National Academy of Sciences, 116, 20309–20314, https://doi.org/10.1073/pnas.1907574116, 2019.

Salter, M. E., Nilsson, E. D., Butcher, A., and Bilde, M.: On the seawater temperature dependence of the sea spray aerosol generated by a continuous plunging jet, Journal of Geophysical Research: Atmospheres, 119, 9052–9072, https://doi.org/10.1002/2013JD021376, 2014.

Salter, M. E., Zieger, P., Acosta Navarro, J. C., Grythe, H., Kirkevåg, A., Rosati, B., Riipinen, I., and Nilsson, E. D.: An empirically derived inorganic sea spray source function incorporating sea surface temperature, Atmospheric Chemistry and Physics, 15, 11047–11066, https://doi.org/10.5194/acp-15-11047-2015, 2015.

Sauer, J. S., Mayer, K. J., Lee, C., Alves, M. R., Amiri, S., Bahaveolos, C. J., Franklin, E. B., Crocker, D. R., Dang, D., Dinasquet, J., Garofalo, L. A., Kaluarachchi, C. P., Kilgour, D. B., Mael, L. E., Mitts, B. A., Moon, D. R., Moore, A. N., Morris, C. K., Mullenmeister, C. A., Ni, C.-M., Pendergraft, M. A., Petras, D., Simpson, R. M. C., Smith, S., Tumminello, P. R., Walker, J. L., DeMott, P. J., Farmer, D. K., Goldstein, A. H., Grassian, V. H., Jaffe, J. S., Malfatti, F., Martz, T. R., Slade, J. H., Tivanski, A. V., Bertram, T. H., Cappa, C. D., and Prather, K. A.: The Sea Spray Chemistry and Particle Evolution study (SeaSCAPE): overview and experimental methods, Environ. Sci.: Processes Impacts, 24, 290–315, https://doi.org/10.1039/D1EM00260K, 2022.

Sellegri, K., Barthelmeß, T., Trueblood, J., Cristi, A., Freney, E., Rose, C., Barr, N., Harvey, M., Safi, K., Deppeler, S., Thompson, K., Dillon, W., Engel, A., and Law, C.: Quantified effect of seawater biogeochemistry on the temperature dependence of sea spray aerosol fluxes, Atmospheric Chemistry and Physics, 23, 12949–12964, https://doi.org/10.5194/acp-23-12949-2023, 2023.

Sofieva, S., Asmi, E., Atanasova, N. S., Heikkinen, A. E., Vidal, E., Duplissy, J., Romantschuk, M., Kouznetsov, R., Kukkonen, J., Bamford, D. H., Hyvärinen, A.-P., and Sofiev, M.: Effects of temperature and salinity on bubble-bursting aerosol formation simulated with a bubble-generating chamber, Atmospheric Measurement Techniques, 15, 6201–6219, https://doi.org/10.5194/amt-15-6201-2022, 2022.

Song, A., Li, J., Tsona, N. T., and Du, L.: Parameterizations for sea spray aerosol production flux, Applied Geochemistry, 157, 105776, https://doi.org/10.1016/j.apgeochem.2023.105776, 2023.

Stokes, M. D., Deane, G. B., Prather, K., Bertram, T. H., Ruppel, M. J., Ryder, O. S., Brady, J. M., and Zhao, D.: A Marine Aerosol Reference Tank system as a breaking wave analogue for the production of foam and sea-spray aerosols, Atmospheric Measurement Techniques, 6, 1085–1094, https://doi.org/10.5194/amt-6-1085-2013, 2013.

Von Der Weiden, S. L., Drewnick, F., and Borrmann, S.: Particle Loss Calculator - A new software tool for the assessment of the performance of aerosol inlet systems, Atmospheric Measurement Techniques, 2, 479–494, https://doi.org/10.5194/amt-2-479-2009, 2009.

Williams, A. S., Dedrick, J. L., Russell, L. M., Tornow, F., Silber, I., Fridlind, A. M., Swanson, B., DeMott, P. J., Zieger, P., and Krejci, R.: Aerosol size distribution properties associated with cold-air outbreaks in the Norwegian Arctic, Atmos. Chem. Phys., 24, 11791–11805, https://doi.org/10.5194/acp-24-11791-2024, 2024.

Zábori, J., Matisāns, M., Krejci, R., Nilsson, E. D., and Ström, J.: Artificial primary marine aerosol production: a laboratory study with varying water temperature, salinity, and succinic acid concentration, Atmospheric Chemistry and Physics, 12, 10709–10724, https://doi.org/10.5194/acp-12-10709-2012, 2012.

Zinke, J., Nilsson, E. D., Zieger, P., and Salter, M. E.: The Effect of Seawater Salinity and Seawater Temperature on Sea Salt Aerosol Production, Journal of Geophysical Research: Atmospheres, 127, https://doi.org/10.1029/2021jd036005, 2022.